




Cite this: *Polym. Chem.*, 2023, **14**, 1275

# Process intensified synthesis of luminescent poly(9,9-dioctylfluorene-*alt*-benzothiadiazole) and polyvinyl alcohol based shape memory polymeric nanocomposite sensors toward cold chain logistics information monitoring

Yuanzuo Zou,<sup>†a,b</sup> Jingzhou Guo,<sup>†a,b</sup> Yinglu Liu,<sup>a,b</sup> Yudi Du,<sup>b</sup> Yuan Pu<sup>b</sup> and Dan Wang  <sup>\*a,b</sup>

Process intensification technologies based on novel reactors have been considered to be the most promising progress paths for developing more efficient chemical processes. In this work, the synthesis of poly(9,9-dioctylfluorene-*alt*-benzothiadiazole), abbreviated as F8BT, was achieved *via* Suzuki cross-coupling polymerization in a rotating packed bed (RPB) reactor maintained in an oxygen-free environment. The synthesized F8BT has a number average molecular weight of 35.2 kDa, a polymer dispersity index of 2.47 and double band absorption and yellow-green photoluminescence properties. An aqueous dispersion of F8BT nanoparticles was then prepared by solvent–antisolvent recrystallization in an external circulation RPB reactor, and spherical nanoparticles with an average particle size of 175.6 nm and a particle dispersion index within 0.2 were obtained. The nanoparticles, which appear yellowish green in color under 365 nm excitation, were uniformly incorporated into polyvinyl alcohol by virtue of the compatibility brought about by hydrogen bonding to obtain PVA composite films containing F8BT nanoparticles. The composite film has a shape memory function, and the irreversible shape change process from the initial “closure” to the final “blooming” is completed in about 15 min at an ambient temperature of 20 °C and 60% relative humidity. It is expected to be used as an optical functional device to monitor the cold chain.

Received 22nd December 2022,  
Accepted 22nd February 2023

DOI: 10.1039/d2py01588a

rsc.li/polymers

## Introduction

Cold chain transportation has been growing rapidly in recent years and plays an important role in the transportation of food, pharmaceuticals and chemicals.<sup>1,2</sup> Temperature monitoring has always been a key part of cold chain transportation.<sup>3–5</sup> As a class of stimuli-responsive polymers, shape memory polymers (SMPs) have the ability to revert from a temporary shape to the initial shape under external stimuli (*e.g.* temperature),<sup>6–9</sup> which is well suited for the temperature monitoring required for cold chain transportation.<sup>10</sup> Incorporating functional materials into shape memory polymers can give them new functionalities that involve changes in stability,<sup>11</sup> biocompatibility,<sup>12</sup> optical properties,<sup>13</sup> and thermal adaptation.<sup>14</sup> In particular, polyvinyl alcohol (PVA)-based shape memory compo-

sites can be used in a wider range of applications due to their simple preparation and induction in water, offering the possibility of more applications.<sup>15–17</sup> By combining PVA with fluorescent nanomaterials, luminescent SMP nanocomposites which can be used as temperature sensors in cold chain transportation can be obtained. Such composites should not only maintain the flexible and sensitive memory function of polymeric materials but also have good fluorescence properties, as well as good compatibility between the fluorescent materials and the matrix polymer.<sup>18–20</sup>

Poly(9,9-dioctylfluorene-*alt*-benzothiadiazole) (F8BT) is a typical organic semiconductor polymer composed of alternating links of 9,9-dioctylfluorene and benzothiadiazoles. The performance of F8BT is mainly controlled by the aromatic conjugated groups and the flexible saturated alkane side chain.<sup>21–25</sup> The F8BT polymers purchased from different chemical suppliers usually show huge variability in performance, with photoluminescence quantum yields (PLQYs) ranging from 7% to 60% in neat films, due to the differences in their molecular weight and polymer dispersity index (PDI). The technological factors effected on the performance of poly-

<sup>a</sup>State Key Laboratory of Organic-Inorganic Composites, Beijing University of Chemical Technology, Beijing 100029, China. E-mail: wangdan@mail.buct.edu.cn

<sup>b</sup>Research Center of the Ministry of Education for High Gravity Engineering and Technology, Beijing University of Chemical Technology, Beijing 100029, China

<sup>†</sup>These authors contributed equally to this work.

mers such as molecular weight, polydispersity and reproducibility, apply equally to F8BT.<sup>26,27</sup> The development of green processes for synthesizing F8BT with precise control at the molecular level for multistep procedures is still at an early stage. Process intensification has been considered to be one of the most promising progress paths for developing more efficient chemical processes. High-gravity technology based on a rotating packed bed (RPB) creates a high gravity environment by the centrifugal force of high-speed rotating packing to achieve uniform concentration and supersaturation at the microscopic scale inside the reactor and is an effective means to intensify liquid-phase reactions and prepare nanoparticles.<sup>28–31</sup> Based on these advantages, RPBs have been shown to be used as process enhancements for the preparation of a variety of materials, such as the preparation of inorganic nanoparticles, polymer precursors, nanoemulsions, *etc.*<sup>32–34</sup> They also have advantages over conventional reactors for the crystallization and purification of organic molecular solvents in an antisolvent.<sup>35</sup> However, to the best of our knowledge, process intensification technologies based on RPB reactors have still not been applied in the synthesis of luminescent F8BT and their performance in the fabrication of shape memory polymeric nanocomposites is a very worthy subject of study.

In this work, we prepared F8BT based on the process intensification technique of a RPB. The  $M_n$  of the obtained product reached 35.2 kDa and the PDI was 2.47. The F8BT nanoparticles with an average size of 175.6 nm and a particle dispersion index of 0.17 were obtained by using a convenient and efficient solvent-resistant recrystallization method enhanced by a RPB. The low size distribution of nanoparticles facilitates the subsequent synthesis of composites. The F8BT nanoparticles were doped into PVA by the hot-casting method and the prepared composite film was named PVA-F8BT. This composite film has excellent transmittance, exhibits yellow light and has good mechanical properties. Based on the optical properties and shape memory effect of PVA-F8BT, a detection switch applied in the cold chain transportation process is designed to monitor whether there is a significant change in temperature during transportation, providing a new idea for cold chain transportation monitoring.

## Experimental

### Materials and instruments

The monomer 2,7-bis(4,4,5,5-tetramethyl-1,3,2-dioxaborolan-2-yl)-9,9-di-*n*-octylfluorene (F8-Bpin) was purchased from Meyer (Shanghai, China). 4,7-Dibromo-2,1,3-benzothiadiazole (BTD) and polyvinyl alcohol (PVA) were obtained from Aladdin (Shanghai, China). Common organic solvents including toluene, dichloromethane ( $\text{CH}_2\text{Cl}_2$ ), tetrahydrofuran (THF), chloroform, methanol, and acetone were purchased from Beijing Chemical Industry Group. Deionized water prepared using a Hitech Laboratory Water Purification System DW100 (Shanghai Hitech Instruments Co., Ltd) was used for all experiments.

A Bruker Avance 400 MHz instrument (400 MHz for  $^1\text{H}$  NMR and 151 MHz for  $^{13}\text{C}$  NMR) was used for the measurement of nuclear magnetic resonance (NMR) spectra by dissolving the sample in deuterated chloroform with tetramethylsilane as a reference. Fourier-transform infrared (FTIR) spectra were recorded on a Bruker Vertex-70v instrument. The  $M_n$  and PDI were determined using gel permeation chromatography (GPC) equipment (Waters 1525 Separation Module) with polystyrene as the standard and trichlorobenzene at 150 °C as the eluent. Ultraviolet-visible (UV-vis) absorbance spectra were measured using a UV-vis spectrophotometer (UV-2600, Shimadzu) and photoluminescence (PL) spectra were recorded using a spectrofluorometer (FS5, Edinburgh). The mechanical tensile properties are mainly reflected by the stress-strain curve determined using a universal testing machine (CMT6503, MTS SYSTEMS).

### Synthesis of F8BT

An internal circulation RPB reactor maintained in an oxygen-free environment was used for the Suzuki cross-coupling polymerization to synthesise F8PT. The apparatus of the RPB reactor used in this work was the same as our previous reports, in which the mixed solution could be passed through the wire mesh packing zone under high gravity. Briefly, 2 mmol F8-Bpin, 2 mmol BTD and 2 mL Aliquat 336 were dissolved in 40 mL toluene and the mixture was added to the RPB reactor followed by the addition of 160 mL deionized water in a nitrogen environment. Then, 180 mL aqueous solution containing 0.02 mol  $\text{K}_2\text{CO}_3$  and 20 mL toluene solution containing 0.14 mmol  $\text{Pd}(\text{PPh}_3)_4$  was injected into the RPB reactor working at a high-gravity of 500 G at 80 °C for 24 h with  $\text{N}_2$  pumped ( $0.2 \text{ L min}^{-1}$ ). After that, methanol was added to the resulting mixture and the precipitate was filtered, re-dissolved in  $\text{CH}_2\text{Cl}_2$  and washed with brine. Anhydrous  $\text{MgSO}_4$  was used to remove residual water and the filtrate was evaporated in a vacuum at 45 °C. The residue was dissolved in THF, added dropwise to methanol and then purified by Soxhlet extraction with acetone to give the product. The final solid of F8BT was obtained after drying under vacuum at 45 °C. The  $M_n$  of the obtained product reached 35.2 kDa and the PDI was 2.47.  $^1\text{H}$  NMR (400 MHz,  $\text{CDCl}_3$ ,  $\delta$ , ppm): 8.11 (br, ArH), 8.06–7.89 (br, ArH), 2.15 (s,  $\text{CH}_2$ ), 1.28–1.17 (br,  $\text{CH}_2$ ), 0.96 (br,  $\text{CH}_2$ ), 0.80 (m,  $\text{CH}_3$ ).

### Preparation of F8BT nanoparticles

The F8BT nanoparticles were prepared by solvent-antisolvent recrystallization in an external circulation RPB reactor. Briefly, 30 mg of F8BT was added to 30 mL THF and kept in a 50 °C water bath under sonication for 5 min to form a clear solution, which was then cooled to 25 °C as the solvent phase. The antisolvent was 480 mL deionized water. Both the solvent and antisolvent were simultaneously pumped into the RPB reactor working at 500 G. The slurry collected from the outlet of the RPB reactor was subjected to rotating evaporation at 50 °C for 30 min and the condensed solution was filtered through a Buchner funnel with a nylon filter membrane ( $0.2 \mu\text{m}$ ). The

powder of F8BT nanoparticles was obtained by freeze-drying treatment of the filtrate.

### Fabrication of the PVA-F8BT nanocomposite

The polymer thin films of the PVA-F8BT nanocomposite were fabricated *via* the solution mixing method followed by a thermal casting method. Briefly, 1.0 g of PVA was added to 10 mL aqueous dispersion of F8BT nanoparticles (0.5 wt%) and magnetically stirred in a water bath at 90 °C for 30 min. The obtained transparent viscous mixture was slowly poured into a clean quartz Petri dish (11 cm in diameter) along the inner wall while it was still hot and spread naturally. After keeping the sample in the dark at room temperature for 5 days, the cured PVA-F8BT film was formed due to sufficient natural drying. Then the polymer thin films were torn off from the Petri dish and were made into different shapes and dimensions by self-designed cutting.

## Results and discussion

The formation of the raw F8BT polymer was achieved based on the typical Suzuki cross-coupling reaction and the main reaction involved is described in Fig. 1a. Toluene was used as the reaction phase with palladium catalysts dissolved in the solution and water acted as the alkali source. The Aliquat 336 added to the reactants produced a marked effect on the reduction of Pd(II) and the stabilization of Pd(0). The inner circulation RPB reactor mainly includes a packing layer and a high-speed rotor, which brings about high-speed rotation and promotes the circulation and contact of the liquid mixture in the reactor. In addition, an inert gas path and a condenser were added to maintain an oxygen-free environment to avoid the deactivation of the palladium catalyst (Fig. 1b). According to the liquid flow characteristics in the RPB reactor, driven by the centrifugal force generated by the high speed rotation of the rotor, the immiscible liquids were continuously torn apart

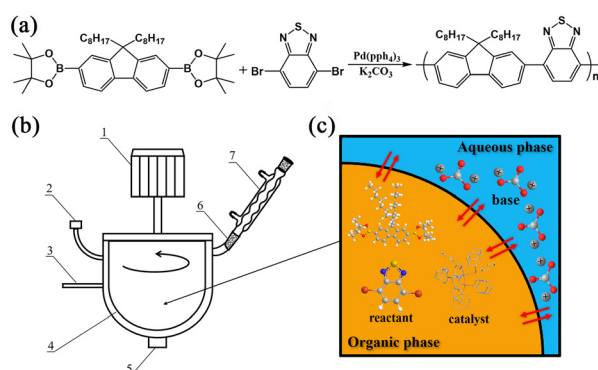


**Fig. 1** (a) Reaction scheme of the synthesis of F8BT *via* the Suzuki cross-coupling reaction. (b) Inner circulation RPB reactor with the following components: 1, rotor; 2, injection inlet; 3, N<sub>2</sub> inlet; 4, thermostatic bath; 5, discharge hole; 6, feed inlet; and 7, condenser. (c) Schematic diagram of the reaction at the interface between organic phase and aqueous phase of the tiny reaction unit of droplet.

and reorganized by the RPB packing layer, which means that the apparent contact between the two phases was constantly renewed (Fig. 1c). Although the F8BT polymer has been widely used for a variety of applications, the commercialized products of F8BT have a low molecular weight (average  $M_n \leq 25\,000$ ) and exhibit huge performance variations depending on the chemical supplier. The homogeneous mixing of reactants at the molecular to nanometer scale is critical for the reaction to obtain the polymer product with the desired molecular weight and molecular weight distribution. Process intensification technologies based on RPB reactors have been proved to be efficient for the production of polymers with uniform structures.<sup>36,37</sup> For the synthesis of F8BT, the RPB reactor also showed a practical value and application prospect. Under the optimized conditions, the F8BT polymer obtained showed an  $M_n$  value of 35.2 kDa and a PDI of 2.47.

Fig. 2a presents the <sup>1</sup>H NMR spectra of the synthesized polymer, and by combining with the FTIR spectral analysis in Fig. 2b, the molecular structure of F8BT was confirmed. The FTIR plots at 2920 cm<sup>-1</sup>, 2846 cm<sup>-1</sup>, and 1456 cm<sup>-1</sup> correspond to the long alkane chain stretching vibration and deformation vibration of the fluorene unit, that at 3030 cm<sup>-1</sup> corresponds to the hydrocarbon on the benzene ring, that near 1547 cm<sup>-1</sup> corresponds to the benzene ring backbone, and that at 650–1000 cm<sup>-1</sup> in the fingerprint area corresponds to the multiple substitutions on the benzene ring. Besides, a C–N characteristic peak appears at 1088 cm<sup>-1</sup>, and that at 1338 cm<sup>-1</sup> may be caused by the C=N stretching vibration on BTB. The TGA curve indicates that F8BT has thermal stability due to the conjugated molecular backbone. As shown in Fig. 2c, F8BT was thermally cleaved at temperatures up to 389 °C (at 5% weight loss) under an inert nitrogen atmosphere. The weight loss of the product starts at about 320 °C at

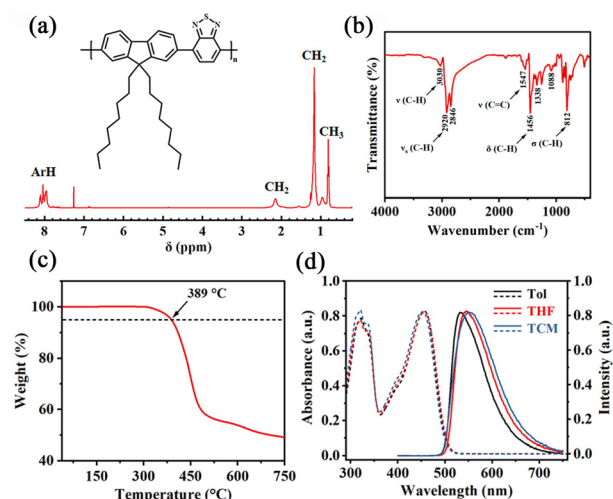


**Fig. 2** (a) <sup>1</sup>H NMR (in CDCl<sub>3</sub>, TMS as calibration) spectra, (b) FTIR spectra and (c) TGA curve of F8BT and (d) UV-vis absorbance spectra (dotted line) and luminescence spectra (solid line) of F8BT solution in toluene (Tol), tetrahydrofuran (THF) and chloroform (TCM) ( $\lambda_{\text{ex}} = 372$  nm).

a heating rate of  $5\text{ }^{\circ}\text{C min}^{-1}$  and remains stable until then. The UV-vis and PL spectra of F8BT in toluene, THF and chloroform are shown in Fig. 2d, all exhibiting approximate double-band absorption and photoluminescence properties. The UV-vis spectroscopy responds to the conjugate length of molecules and reflects the excitation energy required for chromophores of different conjugate types. In toluene, F8BT has absorption peaks triggered by  $\pi\text{-}\pi^*$  transitions at 322 nm and 457 nm, corresponding to the absorption of fluorene units and BTD chromophores, respectively. Similarly, the absorption peaks of F8BT are at 320 nm and 456 nm in THF and 321 nm and 453 nm in chloroform. The PL spectra showed that F8BT in different solutions has a single emission peak in the yellow-green light band, which corresponds to 533 nm in toluene, 544 nm in THF, and 552 nm in chloroform, and the weak red-shift is related to the solvent effect.

Furthermore, a facile and efficient anti-solvent recrystallization method reinforced by a RPB was used to prepare F8BT nanoparticles (Fig. 3a). The nucleation process of nanoparticles can be controlled by a RPB with its strong micro-mixing ability, which ensures a consistent nucleation time and

uniform size distribution of nanoparticles. Generally, for the compatibility of doping units and matrices, the smaller the nanoparticle size, the fuller the resulting composite structure and the higher the added value. Therefore, the experimental conditions were optimized with the goal of keeping the particle size of the nanoparticles as low as possible. During the nucleation, precipitation, and molding of nanoparticles, the degree of supersaturation caused by the mixing of solvents with different solubilities is the key to determining the uniformity of the particle size and morphology. Based on the molecular structure characteristics of F8BT, easily removable and highly soluble THF was chosen as the solvent, and readily available and insoluble water was chosen as the anti-solvent. The volume ratio of THF to water was investigated and optimized in order to determine a relatively suitable supersaturation for mixing the two in a high-gravity environment. F8BT nanoparticles with a size of less than 100 nm were prepared in a RPB (Fig. 3c). DLS measurements show that F8BT nanoparticles dispersed in water have a hydrodynamic diameter of 175.6 nm with a particle dispersion index of 0.17, due to the clumping of tiny nanoparticles in the aqueous medium due to excessive surface energy. Aqueous nanodispersions (0.5 wt%) of F8BT are translucent and fluorescent yellow under 365 nm UV light, which is related to the small size and uniform distribution of nanoparticles (Fig. 3e). The molecular structure of the nanoparticles was further characterized and analyzed. As shown in the FTIR spectra of Fig. 3d, the peaks at  $2920\text{ cm}^{-1}$ ,  $2846\text{ cm}^{-1}$  and  $1456\text{ cm}^{-1}$  are caused by the stretching and deformation vibrations of the C-H bond on the saturated alkane chain. The peaks at  $3030\text{ cm}^{-1}$  and  $1547\text{ cm}^{-1}$  correspond to the stretching vibrations of C-H and C=C on the benzene ring, respectively. In particular, there is a peak at  $1338\text{ cm}^{-1}$  in the spectrum, which is caused by the C=N stretching vibration on benzothiadiazole.

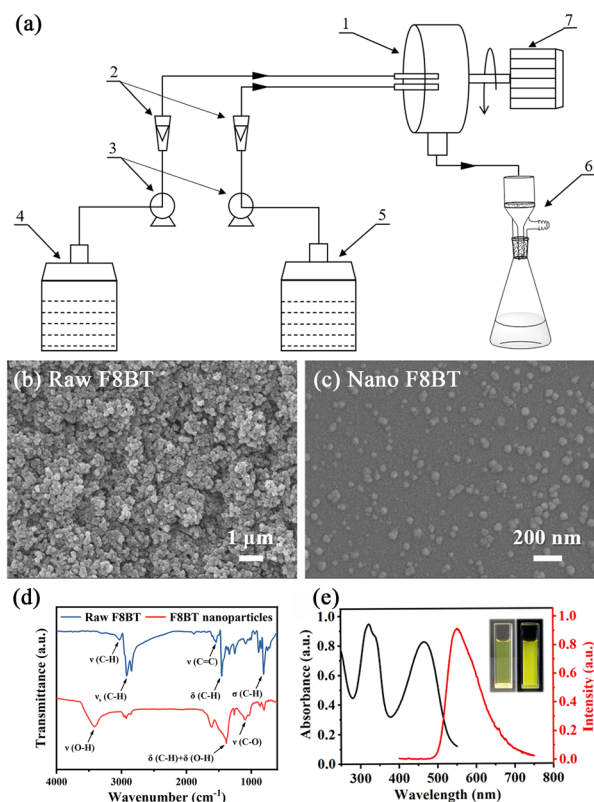


**Fig. 3** (a) External circulation RPB reactor with the following components: 1, reactor; 2, flow meters; 3, pumps; 4, solvent phase storage containers; 5, antisolvent phase storage container; 6, vacuum filters; and 7, rotor. SEM image of (b) raw materials and (c) nanoparticles of F8BT. (d) FTIR spectra of raw F8BT and nanoparticles of F8BT. (e) UV-vis absorbance and luminescence spectra of an aqueous dispersion of F8BT nanoparticles (inset photos were taken under sunlight and 365 nm UV light excitation).

### Fluorescence and mechanical properties of PVA-F8BT films

In the SEM images, nanoparticles are clearly present in the PVA-F8BT membrane section (Fig. 4b) compared to the pristine PVA membrane section (Fig. 4a), indicating effective doping. Due to the abundant hydroxyl groups in the molecular structure, the molecular cross-linked network structure of PVA is dominated by hydrogen bonds, which provides a compatible site for F8BT nanoparticles (Fig. 4c). In the FTIR spectrum of Fig. 4d, PVA-F8BT contains characteristic peaks caused by a large number of hydroxyl groups, including broad peaks in the range of  $3100\text{--}3700\text{ cm}^{-1}$  and so on. On this basis, PVA-F8BT has stronger absorption on the stretching vibration peak of C-H bond at  $3000\text{--}2850\text{ cm}^{-1}$  because of the saturated alkane side chain on the molecular chain of F8BT.

The absorption and emission properties of light are newly added features of the composite films. The absorption peaks of PVA-F8BT films at 322 nm, 335 nm and 465 nm and the emission peaks at 556 nm are close to each other (Fig. 5a). The uniform doping of F8BT nanoparticles in PVA makes PVA-F8BT exhibit yellow light, as can be seen from the photos in the inset. Due to the uniform nanoscale size, the doping amount



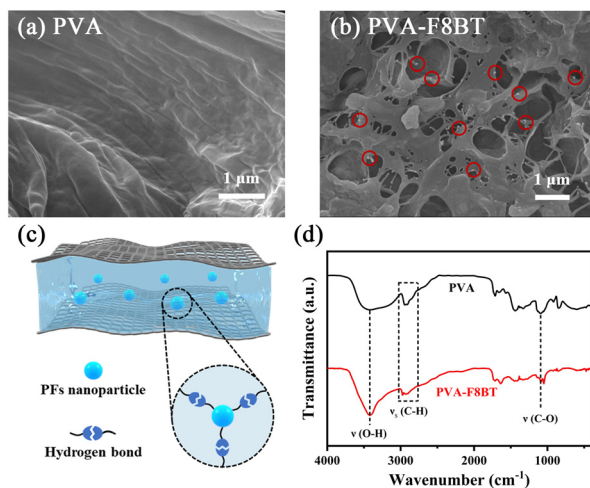


**Fig. 4** SEM images of (a) PVA and (b) PVA-F8BT (the red circles indicate the nanoparticles of F8BT in the composite); (c) schematic diagram of hydrogen bond cross-linking of F8BT nanoparticles in the PVA network structure; and (d) FTIR spectra of PVA and the PVA-F8BT nanocomposite.

can also be changed to achieve flexible tuning for different chromaticities. The dynamic thermodynamic analysis curves of the PVA-F8BT film are shown in Fig. 5b. The energy storage modulus of PVA-F8BT at  $-50\text{ }^{\circ}\text{C}$  is 6188 MPa, which decreases slowly with increasing temperature, starts to drop sharply at  $32.6\text{ }^{\circ}\text{C}$ , and stabilizes after  $80\text{ }^{\circ}\text{C}$  at 100 MPa. Such a large change in modulus indicates that PVA-F8BT has a temperature-controllable unidirectional shape memory capability. After  $50\text{ }^{\circ}\text{C}$ , the energy storage modulus is always larger than the loss modulus, with a peak in the loss factor  $\tan\delta$  at  $54\text{ }^{\circ}\text{C}$ . In PVA-F8BT, PVA undergoes a glass transition. PVA itself has the property of free movement of molecular chains after undergoing the glass transition, and the molecular chains are fixed after lowering the glass transition temperature. The glass transition of PVA occurs at around  $50\text{ }^{\circ}\text{C}$ , while the glass transition temperature increased after doping with F8BT nanoparticles (Fig. 5c), which may be due to the added F8BT producing more hydrogen bonds inside PVA, which affected the glass transition temperature of the whole composite.

Shape-memory polymers can exhibit a variety of shape memory effects and can spontaneously recover the original permanent shape or transform into one or more temporary shapes by virtue of different response levels and response types under appropriate stimuli. As shown in Fig. 6a and b, PVA-F8BT with fluorescence has unidirectional water/thermal induced shape memory properties. The temporary shape of the PVA-F8BT film after softening at elevated temperature and shape-setting at lower temperature is V-shaped and remains unchanged at room temperature, with a shape fixation rate ( $R_f$ ) of about 89%.

$$R_f = \frac{\alpha}{180} \times 100\%$$

where  $\alpha$  is the angle of PVA-F8BT after shape-setting; see Fig. 6a. When immersed in  $50\text{ }^{\circ}\text{C}$  water, the material approaches the glass transition and water molecules penetrate into the hydrophilic cross-linked lattice structure, which directly recovers to a flat, straight shape in 2 min. From a thermodynamic point of view, this shape memory recovery process of PVA-F8BT proceeds through three stages: in the initial state, the polymer molecular chains can be regarded as springs with relatively large lengths and diameters, which are cross-linked and intertwined and mixed together by hydrogen bonds and other intermolecular forces; when the temperature rises, the springs are stretched and rearranged by external effects, and entropy reduction from chaos to order occurs, and stress is stored in the form of elastic potential energy. When the temperature rises again or water molecules flood into the hydrophilic backbone of the cross-linked polymer, the spring acquires thermal viscoelasticity or filling swelling, releasing the elastic potential energy stored inside and causing an irreversible deformation process.

We designed a temperature and humidity monitoring smart switch to meet the special conditions (Fig. 6c) combined with the needs of the monitoring and supervision system of the whole process of cold chain logistics and the shape memory characteristics of PVA-F8BT. This intelligent switch can guarantee a fixed shape at low temperature and low humidity, and will change the energy storage modulus due to dissolution or glass transition once it is exposed to a certain amount of water or high temperature, and irreversible stretching will occur. If

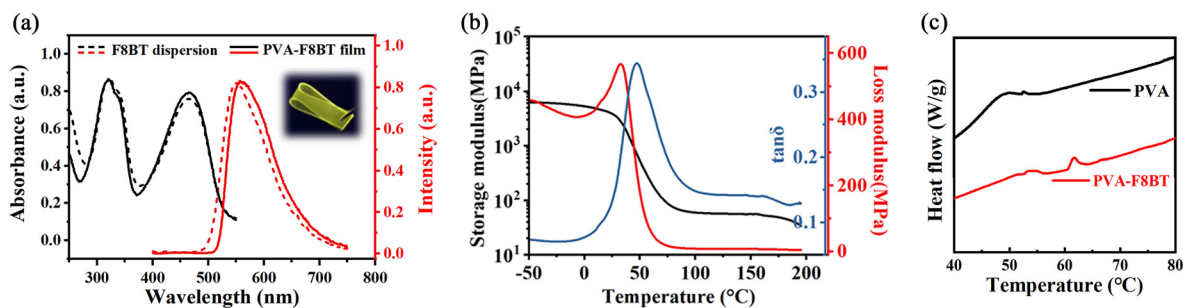


**Fig. 5** (a) UV-vis and luminescence spectra of the F8BT dispersion and the PVA-F8BT film (inset is the photo of the typical PVA-F8BT film under 365 nm UV light excitation); (b) DMA curves of the typical PVA-F8BT film; and (c) DSC curves of PVA and PVA-F8BT.

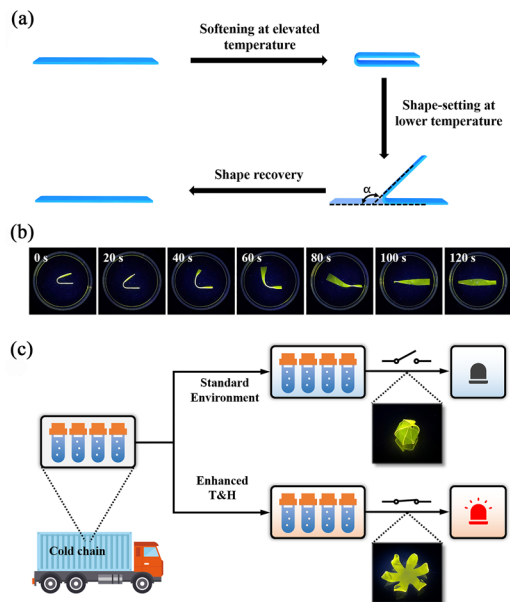


**Fig. 6** (a) Schematic diagram of shape memory behavior. (b) The shape memory recovery behaviour of PVA-F8BT induced by 50 °C water (photos were taken under 365 nm UV light excitation); and (c) schematic diagram and photos of the PVA-F8BT sensor for monitoring the temperature and humidity in cold chain logistics.

the temperature or humidity increases during the cold chain transportation, it will stretch from the original fixed temporary “closed” shape to the final “blooming” shape, and the deformation process will turn on or trigger the monitoring alarm and other devices, which can effectively monitor the whole transportation process. At the same time, the device shows an obvious fluorescence phenomenon under ultraviolet light, which provides a certain guarantee for the supervision of special chemical materials or medical drugs that need to be protected from light, water and high temperature. The PVA-F8BT sample film has been tested to complete the irreversible shape change process from the initial “closure” to the final “blooming” in about 15 min at an ambient temperature of 20 °C and 60% relative humidity.

## Conclusions

In this work, we have efficiently synthesized F8BT with a narrow molecular weight distribution by using a RPB to enhance the Suzuki cross-coupling reaction, and the synthesized F8BT has a number average molecular weight of 35.2 kDa and a PDI of 2.47. Furthermore, the aqueous dispersion of F8BT nanoparticles was prepared by the high-gravity-assisted antisolvent technique, and spherical nanoparticles with an average particle size of 175.6 nm and particle dispersion index within 0.2 were obtained. The nanoparticles retain the fluorescence properties of the  $\pi$  conjugated backbone while adding a new surface hydroxyl functional group, which forms a stable dispersion in water. RPB reactors show

capabilities for process intensified synthesis of luminescent polymers and nanoparticles, which is a kind of complementary technology to microfluidic systems, which allows fast mass transfer and molecular mixing during the reaction, as well as large mass fluxes for scale-up. The F8BT nanoparticles were doped into PVA by the hot-casting method to obtain the PVA-F8BT composite film, and uniform doping of F8BT nanoparticles made the composite film exhibit yellow light. The composite film has a shape memory function, and the irreversible shape change process from the initial “closure” to the final “blooming” is completed in about 15 min at ambient temperature of 20 °C and relative humidity of 60%. It is expected to be used as an optical functional device to monitor the temperature and humidity changes throughout the cold chain.

## Author contributions

D. W conceived and designed this work. Y. Z. and J. G. conducted the experiments and wrote the paper. Y. L. and Y. D. analysed the characterization. All authors participated in the analysis of experimental data and discussion of the results, as well as in the writing and revision of the manuscript.

## Conflicts of interest

The authors declare no competing financial interest.

## Acknowledgements

We are grateful for the financial support from the National Key Research and Development Program of China (2021YFC3001602).

## References

- X. He, X. W. Liu, P. Li, P. P. Wang, H. J. Cheng, W. Q. Li, B. D. Li, T. Liu and J. Ma, *Engineering*, 2022, **9**, 13–16.
- J. W. Han, M. Zuo, W. Y. Zhu, J. H. Zuo, E. L. Lu and X. T. Yang, *Trends Food Sci. Technol.*, 2021, **109**, 536–551.
- J. J. Zhao, J. L. Long, Y. Q. Du, J. K. Zhou, Y. D. Wang, Z. P. Miao, Y. L. Liu, S. G. Xu and S. K. Cao, *J. Colloid Interface Sci.*, 2020, **564**, 286–295.
- Y. Zhao, X. L. Zhang and X. F. Xu, *J. Therm. Anal. Calorim.*, 2020, **139**, 1419–1434.
- Q. Lin, Q. H. Zhao and B. Lev, *Eur. J. Oper. Res.*, 2020, **283**, 182–195.
- J. J. Shang, X. X. Le, J. W. Zhang, T. Chen and P. Theato, *Polym. Chem.*, 2019, **10**, 1036–1055.
- A. V. Menon, G. Madras and S. Bose, *Polym. Chem.*, 2019, **10**, 4370–4388.
- F. Momeni and J. Ni, *Engineering*, 2020, **6**, 1035–1055.
- N. Yenpech, V. Intasanta, K. Tashiro and S. Chirachanchai, *Polym. Chem.*, 2020, **11**, 91–101.

- 10 Y. L. Xia, Y. He, F. H. Zhang, Y. J. Liu and J. S. Leng, *Adv. Mater.*, 2021, **33**, 2000713.
- 11 T. Koga, K. Tomimori and N. Higashi, *Macromol. Rapid Commun.*, 2020, **41**, 1900650.
- 12 L. Y. Sun, X. Gao, D. C. Wu and Q. Y. Guo, *Polym. Rev.*, 2021, **61**, 280–318.
- 13 A. Belmonte, M. P. da Cunha, K. Nickmans and A. Schenning, *Adv. Opt. Mater.*, 2020, **8**, 2000054.
- 14 W. S. Miao, W. K. Zou, Y. W. Luo, N. Zheng, Q. Zhao and T. Xie, *Polym. Chem.*, 2020, **11**, 1369–1374.
- 15 Y. Y. Han, H. M. Wang, X. L. Jiao and D. R. Chen, *J. Appl. Polym. Sci.*, 2020, **137**, 49158.
- 16 S. S. Wu, W. Li, W. Zhou, Y. Zhan, C. F. Hu, J. L. Zhuang, H. R. Zhang, X. J. Zhang, B. F. Lei and Y. L. Liu, *Adv. Opt. Mater.*, 2018, **6**, 1701150.
- 17 P. Yang, Z. Q. Zhu, X. H. Li, T. Zhang, W. Zhang, M. Z. Chen and X. Y. Zhou, *J. Alloys Compd.*, 2020, **834**, 154399.
- 18 A. Cosgun, R. L. Fu, W. N. Jiang, J. H. Li, J. Z. Song, X. H. Song and H. B. Zeng, *J. Mater. Chem. C*, 2015, **3**, 257–264.
- 19 H. Zhi, X. Fei, J. Tian, M. Z. Jing, L. Q. Xu, X. Y. Wang, D. M. Liu, Y. Wang and J. Y. Liu, *J. Mater. Chem. B*, 2017, **5**, 5738–5744.
- 20 H. Y. Zhang, J. X. Liu, F. Shi, T. C. Li, H. J. Zhang, D. Y. Yang, Y. Li, Z. W. Tian and N. Zhou, *Chem. Eng. J.*, 2022, **431**, 133353.
- 21 M. Mbarek, M. M. Almoneef, Y. B. Salah and K. Alimi, *Spectrochim. Acta, Part A*, 2020, **240**, 118502.
- 22 X. Y. Zhang, Z. R. Xu, Y. Zhang, Y. W. Quan and Y. X. Cheng, *J. Mater. Chem. C*, 2020, **8**, 15669–15676.
- 23 M. Sachs, H. Cha, J. Kosco, C. M. Aitchison, L. Francas, S. Corby, C. L. Chiang, A. A. Wilson, R. Godin, A. Fahey-Williams, A. I. Cooper, R. S. Sprick, I. McCulloch and J. R. Durrant, *J. Am. Chem. Soc.*, 2020, **142**, 14574–14587.
- 24 H. R. Zhang, L. L. Ma, Q. Zhang, Y. P. Shi, Y. T. Fang, R. D. Xia, W. Hu and D. D. C. Bradley, *Adv. Opt. Mater.*, 2020, **8**, 1901958.
- 25 B. Borges, A. G. Veiga, M. Gioti, A. Laskarakis, L. Tzounis, S. Logothetidis and M. L. M. Rocco, *Polym. Int.*, 2018, **67**, 691–699.
- 26 Q. Zhang, Q. Wei, X. R. Guo, G. Hai, H. Z. Sun, J. W. Li, R. D. Xia, Y. Qian, S. Casado, J. R. Castro-Smirnov and J. Cabanillas-Gonzalez, *Adv. Sci.*, 2019, **6**, 1801455.
- 27 M. Mamada, R. Komatsu and C. Adachi, *ACS Appl. Mater. Interfaces*, 2020, **12**, 28383–28391.
- 28 C. C. Lin, Y. P. Lai and K. Y. Wu, *Powder Technol.*, 2022, **395**, 369–376.
- 29 J. Xie, X. B. Jia, D. Wang, Y. J. Li, B. C. Sun, Y. Luo, G. W. Chu and J. F. Chen, *Chin. J. Chem. Eng.*, 2022, **48**, 116–124.
- 30 J. T. Du, J. Shi, Q. Sun, D. Wang, H. Wu, J. X. Wang and J. F. Chen, *Chem. Eng. J.*, 2020, **382**, 122883.
- 31 Y. Cai, G. W. Chu, Y. Luo, M. J. Su, B. J. Wang, B. C. Sun and J. F. Chen, *Engineering*, 2021, **7**, 1603–1610.
- 32 B. T. Lu, X. K. Lv and Y. Le, *Polymers*, 2019, **11**, 304.
- 33 Y. Pu, L. F. Lin, J. Liu, J. X. Wang and D. Wang, *Chin. J. Chem. Eng.*, 2020, **28**, 1744–1751.
- 34 X. Z. Liu, C. B. Fu, M. T. Wang, J. X. Wang, H. K. Zou, Y. Le and J. F. Chen, *Chin. J. Chem. Eng.*, 2022, **46**, 94–103.
- 35 J. Guo, J. Yang, Y. Zou, Y. Pu and D. Wang, *J. Chem. Eng. Data*, 2022, **67**, 3310–3316.
- 36 X. Z. Liu, J. S. Jin, Y. L. Chen, T. Lu, Q. Sun, J.-X. Wang, J.-F. Chen and Y. Le, *Chem. Eng. J.*, 2020, **379**, 122400.
- 37 Y. Zou, D. Wang, J. Guo, J. Yang, Y. Pu and J.-F. Chen, *Polym. Chem.*, 2022, **13**, 3506–3512.